Electronic Scan Strategy for Phased Array Weather Radar Using a Space–Time Characterization Model

CUONG M. NGUYEN

Flight Research Laboratory, National Research Council Canada, Ottawa, Ontario, Canada

V. CHANDRASEKAR

Colorado State University, Fort Collins, Colorado

(Manuscript received 13 January 2016, in final form 27 January 2017)

ABSTRACT

This paper presents an adaptive scan strategy concept for phased array weather radars (PAWR) with the objective of increasing the scan speed and capturing features of the storm system while maintaining the measurement accuracy. The adaptive scan strategy is developed based on the space–time variability of the storm under observation. Quickly evolving regions are scanned more often and the spatial sampling resolution is matched to the spatial scale. A model that includes the interaction between space and time is used to extract spatial and temporal scales of the medium and to define scanning regions. The temporal scale constrains the radar revisit time, while the measurement accuracy controls the radar's dwell time. These conditions are employed in a task scheduler that works on a ray-by-ray basis and is designed to balance task priority and radar resources. The scheduler algorithm also includes an optimization procedure for minimizing radar scan time. The model and the scan strategy are demonstrated using simulation data. The results show that the proposed scan strategy can reduce the scan time significantly without compromising data quality.

1. Introduction

Following the success of the WSR-88D network, considerable effort has been directed toward exploring options for the next generation of weather radar technology. With its superior capability for rapidly scanning the atmosphere, the electronically scanned phased array radar (PAR) is a potential candidate (Zrnić et al. 2007). The advantage of PAR compared to conventional weather radar systems is its capability of electronically steering the beam. Conventional weather radars scan the 3D volume by rotating the antenna at some predefined elevation angles known as volume coverage patterns (VCP) and need an update time of 4–6 min for a scan to provide estimated parameters within the required accuracy (ROC 2007). However, fast updates are not always possible with such radar systems due to the inertia of their mechanically rotated antennas. In contrast, PAR can instantly steer the beam to a region of interest. This property of PAR provides faster update times without compromising data quality. First, only precipitation regions are scanned; regions with no echo or insignificant data are skipped (Heinselman et al. 2008). Second, the electronic beam steering capability of PAR allows for scanning and revisiting many regions in a sequence (Yu et al. 2007). This increases the number of independent samples within an integration cycle and requires fewer samples to maintain good data quality. Short update times are critical for better understanding storm structures as well as forecasting them, especially for quickly evolving systems. Rasmussen et al. (2000) suggested that update times of 20–30 s are necessary to resolve the evolutionary processes in tornado genesis. In addition, with PAR, the regions that evolve faster can be scanned more often, a feature that is limited on mechanically scanning radar. Thus, PAR is an excellent platform for precisely capturing the features of storm systems when compared to conventional weather radars.

The benefit of PAR for weather observation is clear. Its capability opens a new era in scanning strategies for weather radars while bringing more challenges to the design. For any phased array radar, the scan strategy is integral, since it is designed to command the radar to

Corresponding author e-mail: Cuong M. Nguyen, cuong.nguyen@nrc-cnrc.gc.ca

DOI: 10.1175/JTECH-D-16-0021.1

scan, track, and perform surveillance. It ensures that the system is working optimally. A scan strategy of a phased array radar is designed based on the features and properties of the radar target and the goal of the sensing. The target of phased array weather radars (PAWR) is weather, a volume target, which is very different from a point target in many respects. Fundamentally, weather consists of a large number of precipitation particles distributed over a large volume evolving in both spatial and temporal dimensions. Moreover, weather radars not only detect but also measure volume targets accurately. Such capabilities mandate specific requirements and algorithms. Recently, Reinoso-Rondinel et al. (2010) introduced a PAWR scheduling algorithm that can arrange scanning and surveillance tasks without significant delays. In that work, targets are treated as individual storm cells and task times are defined as the times to complete scanning the cells. Dynamic evolution parameters of a storm are not automatically extracted and integrated into the scan strategy algorithm, and update times are chosen based on the user's experience; therefore, in general, update times are not optimized for efficiency.

For observing precipitation, three governing factors must be considered: spatial sampling, temporal updating, and measurement accuracy. It is well known that storms exhibit a wide range of variability in both their spatial distribution of intensity and temporal evolution. For example, a tornado can touch down in a highly localized swath of few hundred meter width over a few minutes, while a hurricane can span many hundred kilometers in spatial extent and evolve over days or weeks. To characterize the space–time variability features of a storm system, an integrated space–time model is studied that explicitly includes the interaction between space and time. The model assumes that a storm system is a combination of advection and evolution processes. A procedure is developed to separate these two processes and to estimate the spatial scales present in the storm. By applying the model to a sequence of radar observations, a storm can be segmented into different scanning regions corresponding to each estimated spatial scale. Next, evolution times (or temporal scales) of these regions can be derived from their 2D correlation function. The storm's spatial scales will determine the spatial sampling resolution of the radar, while the evolution time of each region will specify the radar temporal update. Additionally, the accuracy of precipitation measurements at each spatial location is a function of signal parameters at that position (Bringi and Chandrasekar 2001). For a given level of accuracy, that relationship provides a constraint on the dwell time of PAWR at each beam location.

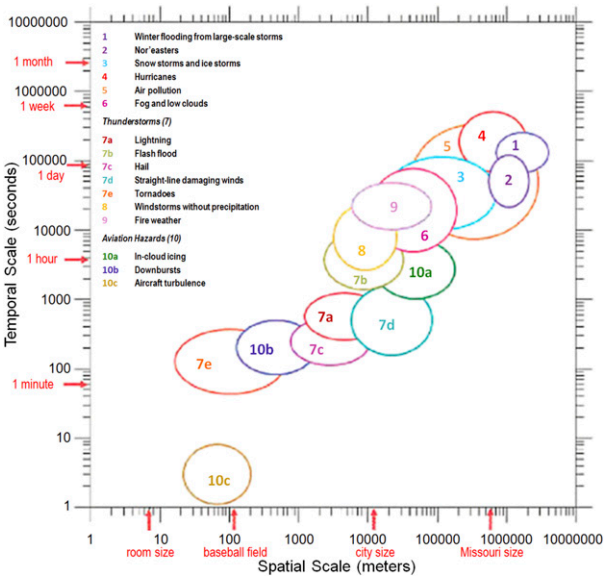

FIG. 1. Time and space scales associated with "high impact" weather phenomena. (Courtesy: National Research Council 2009).

The paper is organized as follows. The space–time model and the estimation of spatial scales present in the storm along with their evolution times are described in section 2. Section 3 proposes a scheme of radar scanning regions for PAWR. A measurement error model for a block pulsing scheme is introduced in section 4. In section 5, requirements and considerations for an adaptive scan strategy are addressed and discussed. This section also contains an optimized scheduling algorithm for the PAWR, and an example of its implementation with a comparison of results to mechanically steered beam weather radar is introduced. Section 6 summarizes the main results of this work.

2. Space–time characterization model for precipitation

a. *Spatial scales in precipitation systems*

Figure 1 presents a relative scale map for different high-impact weather phenomena, exhibiting the connection between space scales and time scales. The figure shows that for precipitation, the temporal scale of a specific region generally increases with its spatial scale. This suggests that knowing the spatial scales present in the storm system will provide some bounds to its temporal scales.

1) AN ALGORITHM FOR SPATIAL-SCALE ESTIMATION

In general, a radar observation includes features over a wide range of spatial scales and to detect and

estimate them is a challenging task. One way of tackling this problem is to consider all possible scales. According to the Nyquist theorem, the smallest resolvable scale in the observation is equal to twice the grid spacing, while the largest scale can be as large as the size of the storm. However, this approach requires considerable processing time and makes the algorithm complex. For the purpose of designing a radar scan strategy, we focus on identifying a small set of significant scales present in the storm.

When applying an averaging filter to a radar observation, the filter's sliding window size (filter size) affects the scales present in the output field. A filter with a larger sliding window removes smaller spatial-scale features, while a filter with a smaller sliding window retains smaller scales. Thus, information about the scales can be extracted from filtered fields using different filter sizes. One way to determine the scales to be retained is to compare the original observation to the output of the filter. The comparison can be quantified using similarity measures, such as Euclidean distance, Mahalanobis distance, and normalized cross correlation. Results from our study show that since the correlation measurement yielded the best results in terms of accuracy and robustness for radar reflectivity observations, that measure was employed in this work. The correlation similarity measure of two radar fields Z_i and Z_j (of sizes $N_1 \times N_2$) is defined as

$$R(Z_i, Z_j) = \frac{1}{N_1}\frac{1}{N_2}\frac{\left|\sum_{l=1}^{N_1}\sum_{k=1}^{N_2}[Z_i(l,k)-\mu_i][Z_j(l,k)-\mu_j]\right|}{\sqrt{\sum_{l=1}^{N_1}\sum_{k=1}^{N_2}[Z_i(l,k)-\mu_i]^2\sum_{l=1}^{N_1}\sum_{k=1}^{N_2}[Z_j(l,k)-\mu_j]^2}},$$
$$\mu_n = \frac{1}{N_1}\frac{1}{N_2}\sum_{l=1}^{N_1}\sum_{k=1}^{N_2} Z_{i,j}(l,k). \quad (1)$$

The normalized cross correlation [Eq. (1)] is inversely proportional to the size of the filter because increasing the filter size removes more scales. To detect and estimate significant scales, we calculated the correlation similarity measure between the original field and filtered fields as a function of filter sizes. It was noticed that the absolute value of the derivative of the similarity measure function attained its local maximum when a characteristic scale was removed from the original field provided the characteristic scale was between the sizes of the two filters. Thus, if the spacing between two filter sizes is sufficiently small, then the characteristic scale can be approximated. Hence, the absolute value of the derivative of the similarity measure function (calculated by finite differences) is a local maximum at the location of a characteristic scale. This idea can be expanded to find all the characteristic spatial scales within a radar observation. In summary, an algorithm to find characteristic special scales present in a radar observation is described by the following steps:

1) A vector of spatial scale candidates is Preset for each radar observation. The minimum scale in the vector is chosen to be equal to twice the data grid spacing, while the maximum scale is set to be equal to the size of the major axis of the storm. In addition, the scale's step is equal to half of the radar grid spacing.
2) An averaging filter with filter size equal to the first scale in the vector (step 1) is applied to the original observation and yields the first filtered field. This process is repeated with the other scales in the vector.
3) Compute a sequence of the normalized cross-correlation values between the original field and the filtered fields (cross correlation as a function of scale).
4) Compute the absolute value of the finite difference of the correlation function (from step 3).
5) Find the first local maximum and its corresponding spatial scale. This scale is considered as an estimated characteristic spatial scale of the radar observation.
6) Filter the original observation by an averaging filter with the filter size equal to the scale found in step 5 and replace the original observation with this filtered field.

Steps 2–6 are repeated until no other characteristic scales are found.

2) PERFORMANCE EVALUATION

The performance of the scale estimation algorithm developed in the previous section is illustrated using simulation. Figure 2 shows a test image consisting of a tiled checkerboard. This image shows two major scales, the size of the smaller checkerboard squares at 25 pixels and the size of the larger checkerboard squares at 50 pixels.

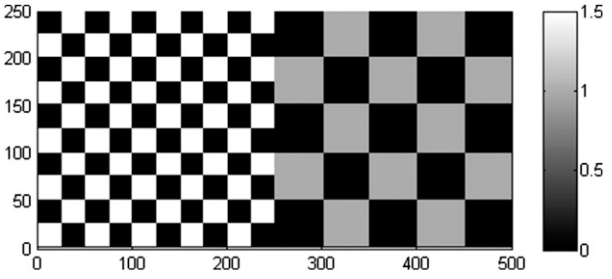

FIG. 2. A synthesized checkerboard image. The size of the smaller checkerboard squares is 25 pixels and the size of the larger checkerboard squares is 50 pixels. Pixel values range from 0 to 1.5.

The initial scale vector is chosen as [2:1:50] pixels for this particular image. In this study, 2D Gaussian filter kernels are used. A 2D Gaussian filter at location (x, y) has the form

$$G_{(x,y)}(u,v;s) = \frac{1}{2\pi s^2} e^{-[(u-x)^2+(v-y)^2/2s^2]}, \qquad (2)$$

where (u, v) are spatial variables. The size of this Gaussian filter is determined by its standard deviation parameter s; for that reason, s is also considered as the "scale" of the filter.

Figure 3a shows the discrete approximation of the derivative of the cross-correlation function with respect to the scale for the first iteration of the algorithm. A local maximum is found at scale 10 pixels. Correspondingly, it is the first estimated significant scale. The algorithm is continuously processed and one more scale is detected at 21 pixels (Fig. 3b) in the second iteration. After this step, no further scale is found. In this type of application, the goal is not to find absolutely accurate estimates but to specify the scales that well represent important structures of the image. Figures 3c and 3d depict the size of the Gaussian averaging filters corresponding to the estimated scales. Visually, they match well to the checkerboard titles in Fig. 2.

b. Data model

Storms generally consist of many features at different spatial scales, moving and evolving over time. Distinguishing between quickly and slowly evolving regions within a storm and estimating temporal scales of these regions are keys in designing an efficient scan strategy. To overcome the design challenges, a space–time characterization model that includes the interaction between space and time for the precipitation system is proposed.

The weather radar observations $Z(x_1, y_1, t_1)$, $Z(x_2, y_2, t_2)$,... are sampled from the underlying field $Z(x, y, t)$,

$$Z(x,y,t) = X(x,y,t) + e(x,y,t), \qquad (3)$$

where (x, y) is the location, t is the sampling time, $X(x, y, t)$ is the reflectivity field, and $e(x, y, t)$ is the measurement uncertainty.

A storm system is a complex physical process. In general, there are two mechanisms involved in a storm process: 1) the storm is constantly moving in the spatial domain and 2) the storm evolves (growth or dissipation) over time. To obtain the temporal scales associated with different spatial scales, it is desired to decompose the storm motion and the storm evolution processes. The motivation behind this is to establish a technique to characterize the storm evolution with the storm motion pattern removed. Over a short period of time (in order

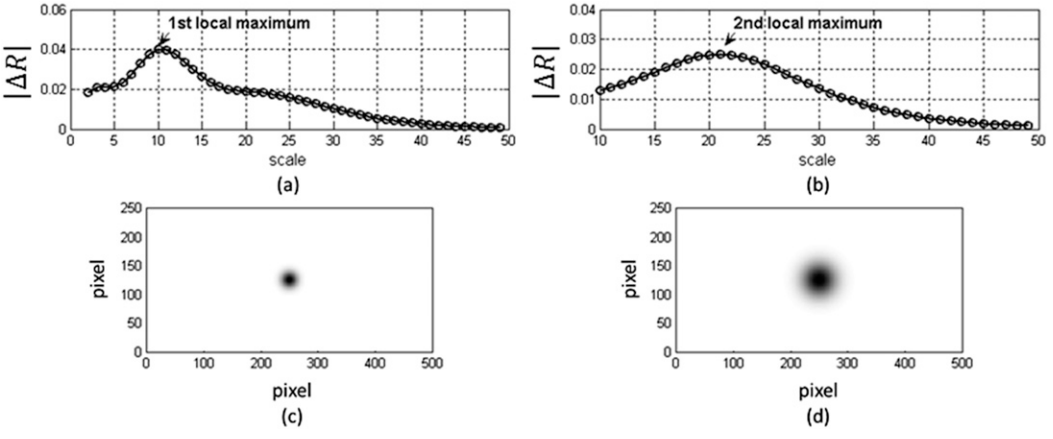

FIG. 3. Results of the spatial-scale estimation algorithm when applying to the simulated data in Fig. 2. The derivatives of the cross-correlation function at the (a) first and (b) second iterations show local maxima at a scale of 10 and 21 pixels. (c),(d) The 2D isotropic Gaussian filters with the standard deviation parameter of 10 and 21 pixels, respectively.

of minutes), we assume that the two processes are independent. The motion process can be presented by a general flow system equation,

$$\frac{\partial}{\partial t}X(x,y,t) = -U(x,y)\frac{\partial}{\partial x}X(x,y,t) - V(x,y)\frac{\partial}{\partial y}X(x,y,t) + S(x,y,t), \quad (4)$$

where $U(x, y)$ is the x-axis motion velocity and $V(x, y)$ is the y-axis motion velocity over the spatial domain. The growth/decay term is represented by $S(x, y, t)$.

The motion field (U, V) of the storm system can be estimated by solving the system of Eq. (4) (Gang and Chandrasekar 2005). Once the motion fields are obtained, they can be removed from the radar observations $X(x, y, t)$ by using an advection algorithm (Rood 1987) to yield the motion-aligned observations denoted by $Y(x, y, t)$. It is assumed that within a short time period, the motion at each observation time is the same. Using the estimated motion field, the image at time "t" is extrapolated to time "$t + 1$" and the result is spatially aligned with the measurement at time "$t + 1$." In general, we can align all the radar precipitation fields with reference to a certain temporal point.

The motion-aligned fields then are used to characterize the storm evolution. The evolution process can be represented by a kernel dilation model (Wikle 2002),

$$Y(x,y;t) = \gamma\int_D k_{(x,y)}(u,v)Y(u,v;t-1)\,du\,dv + \eta(x,y;t), \quad (5)$$

where D denotes the spatial domain, $k_{(x,y)}(u, v)$ is the kernel function at spatial location (x, y), γ is the evolution control factor, and $\eta(x, y, t)$ is the spatially independent colored/white noise.

The dilation kernel function can be approximated by a linear sum of radial basis functions (Park and Sandberg 1991). In this work, the Gaussian radial basis functions [Eq. (2)] are used and the kernel function is expressed as

$$k_{(x,y)}(u,v) = \sum_i \beta_i(x,y)G_{(x,y)}(u,v;s_i), \quad (6)$$

where $\beta_i(x, y) \geq 0$ is the weight corresponding to the Gaussian kernel $G_{(x,y)}(u, v; s_i)$ at location (x, y). Assuming there are M spatial scales present in the observations, the sum in Eq. (6) is truncated at M. Upon substitution of Eq. (6) into Eq. (5), we get a linear model,

$$\begin{cases} \alpha_1(x,y)Y_{1,1}(x,y) + \alpha_2(x,y)Y_{1,2}(x,y) + \cdots + \alpha_M(x,y)Y_{1,M}(x,y) = Y_2(x,y) \\ \alpha_1(x,y)Y_{2,1}(x,y) + \alpha_2(x,y)Y_{2,2}(x,y) + \cdots + \alpha_M(x,y)Y_{2,M}(x,y) = Y_3(x,y) \\ \qquad\qquad\qquad\qquad\qquad\qquad\qquad\qquad\qquad\qquad \vdots \\ \alpha_1(x,y)Y_{N,1}(x,y) + \alpha_2(x,y)Y_{N,2}(x,y) + \cdots + \alpha_M(x,y)Y_{N,M}(x,y) = Y_N(x,y) \end{cases} \quad (7)$$

$$Y_{n,i}(x,y) = \int_D G_{(x,y)}(u,v;s_i)Y_n(u,v)\,du\,dv$$

$$Y_n(x,y) = Y(x,y;n),$$

where N is the number of observations, n is the discrete sampling time stamp, and $\alpha_i = \gamma\beta_i$. When the number of observations is no smaller than the number of spatial scales, that is, $N \geq M$, Eq. (7) forms an overdetermined linear system and can be solved by standard methods, such as the linear least squares estimator (Lawson and Hanson 1987).

It is noticed that the term $Y_{n,i}(x, y)$ [Eq. (7)] is the convolution between a Gaussian kernel of s_i with the observation $Y_n(x, y)$; therefore, it contains only features with spatial scales equal to or larger than s_i. From Eq. (7) one can interpret the weight α_i as an evolution indicator of the feature related to s_i (called the feature of scale s_i). Term $\alpha_i > 1$ indicates that the s_i grows and $\alpha_i < 1$ indicates that the feature of s_i decays. Thus, the distribution of α_i will tell us about the growth and decay regions of s_i. In designing a scan strategy, regions with smaller α_i (decay quickly) will be neglected because it is more important for the radar to detect and track developing hazardous events; hence, s_i can be segmented by simply thresholding the α_i field. Mapping this region to each radar observation $Y_n(x, y)$ $(n = 1, \ldots, N)$ a sequence of measurements for s_i is obtained. The temporal scale associated with s_i is then simply calculated as the time when the 2D correlation function [Eq. (1)] of the sequence drops below a set threshold. A high threshold value ensures that the regions are approximately stationary within the dwell time. In this work, we define the threshold to be 0.9. Smaller temporal scales indicate quick evolution and vice versa.

To illustrate the space–time characterization model described above, we apply it to radar data from a simulation (Tripoli and Büker 2012) demonstrating tornado

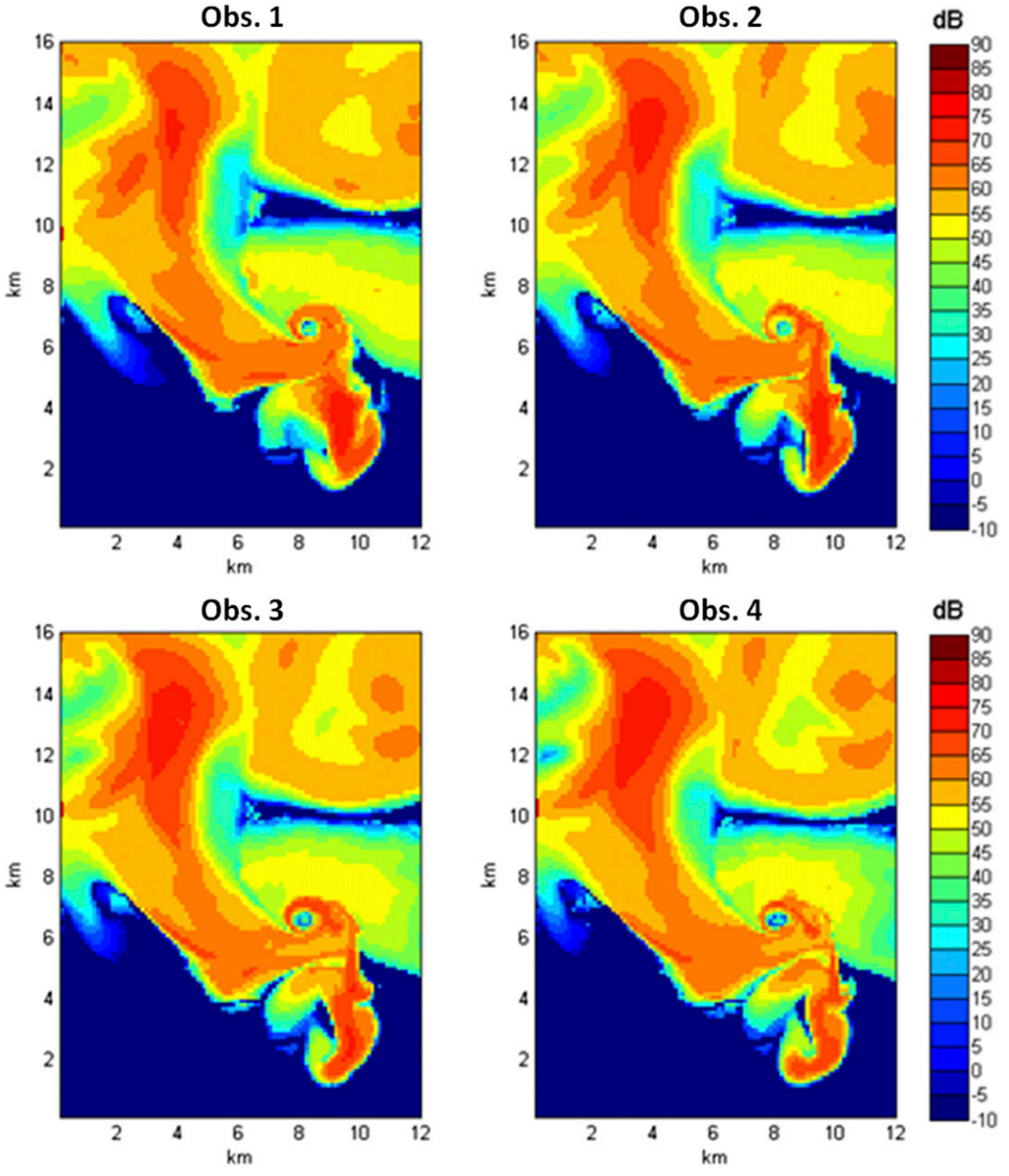

FIG. 4. Simulated consecutive reflectivity factor fields of a tornado development. The spatial sampling resolution is 120 m on both the x and y axes, and the temporal spacing between each observation is 30 s.

development. Figure 4 shows four consecutive radar reflectivity factor fields at height 1 km above the ground. The spatial sampling resolution is 120 m on both the x and y axes, and the temporal spacing between each observation is 30 s. For these simulated fields, no storm motion process is included; therefore, the fields are already motion aligned. The figures show that there is a fast development of the small features around the vortex of the tornado, while the structures of the nearby regions seem to change more slowly.

The scale estimation algorithm (section 2a) is applied to each reflectivity field. For each field, two significant spatial scales are found. The estimated spatial scales for the four simulated fields are (0.42, 1.15), (0.50, 1.26), (0.61, 1.41), and (0.57, 1.37) km. To find common spatial scales representing all four fields, the estimated scales are averaged with results (0.525, 1.297) km. Substituting these scales into Eq. (7) we obtain a system of four linear equations and two unknowns that can be solved by the linear least squares method (Lawson and Hanson 1987).

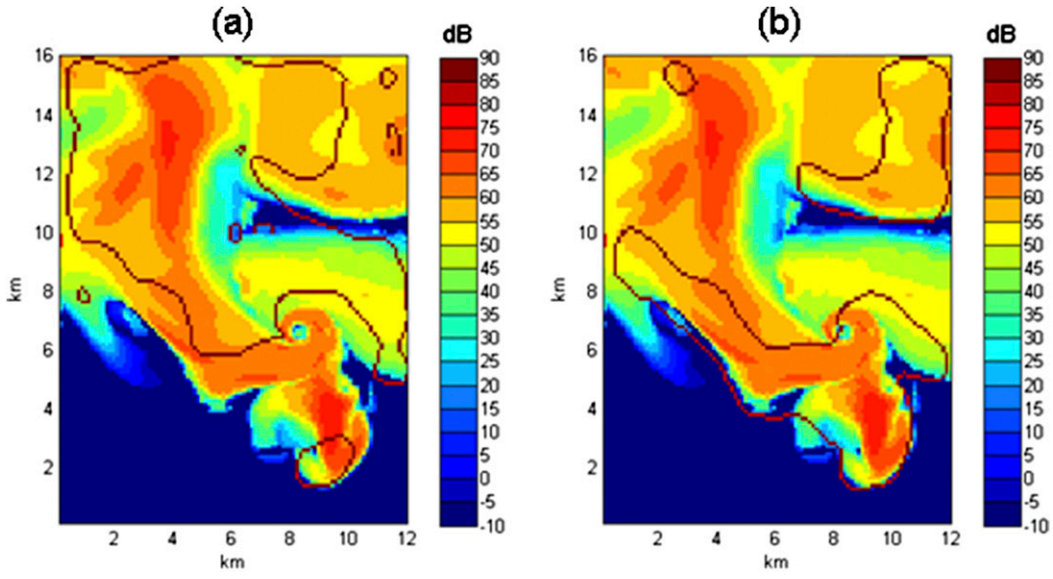

FIG. 5. Segmentation of the tornado (Fig. 4) based on its spatial-scale features: (a) region 1 with a major spatial scale of 1.297 km and (b) region 2 with a major spatial scale of 0.525 km.

Regions corresponding to the two estimated spatial scales are separated by contours (Fig. 5). It can be seen that the region of the main updraft and forward flank downdraft near the tornado vortex circulation and the region of rear flank downdraft where the smaller scale features are prominent are successfully localized (Fig. 5b). The evolution times of the two regions are shown in Fig. 6. It is shown that the region near the tornado vortex (corresponding to the smaller scale, 0.48 km) evolves faster with a decorrelation time of 0.159 min, while the other region develops more slowly with a decorrelation time of 0.274 min. This result is consistent with our hypothesis of the space–time variability of weather systems, where small-scale features evolve more quickly than large-scale features.

3. Radar scanning regions

The space–time characterization model provides a framework for segmenting a storm into different regions based on its space–time variability features. Each region is represented by a unique spatial and temporal scale. At this point, the model is developed only for 2D data. In practice, PAWR is designed to scan the precipitation volume in both azimuth and elevation dimensions. The adaptive scan strategy could be optimized for both directions. It requires the model be modified to work with 3D data, which is beyond the scope of the present work. We therefore simplify the task by optimizing the scan strategy for each elevation angle. The outputs of the adaptive scheduler will be a sequence of azimuth angles where the radar beam will be located to obtain optimal measurements.

Without the loss of generality, only a single-aperture PAWR is considered and we assume that the radar scan domain is limited to a 120° sector. The radar scanning region scheme (Fig. 7) within a storm varies constantly due to a storm's evolution over time and can be also very different between storms, but in general it can be grouped into three categories: separated, partially overlapped, and completely overlapped. In the first case, where scanning regions are separated (Fig. 7a), no further processing is required before information is fed to the scheduler. A case of partial overlapping is shown in Fig. 7b. The azimuthal boundaries of the overlapping region are indicated by dashed lines. The spatial scale

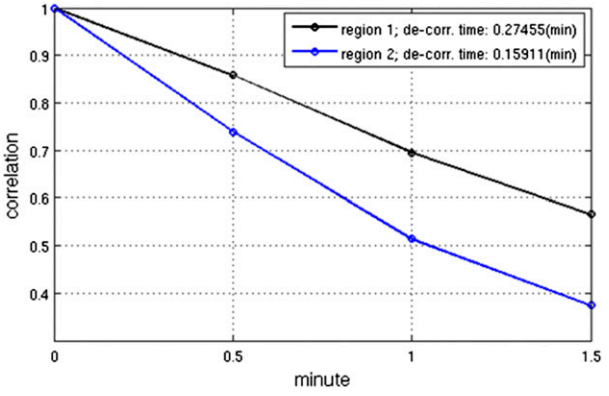

FIG. 6. Correlation functions of the two regions in the tornado simulated data (Fig. 5).

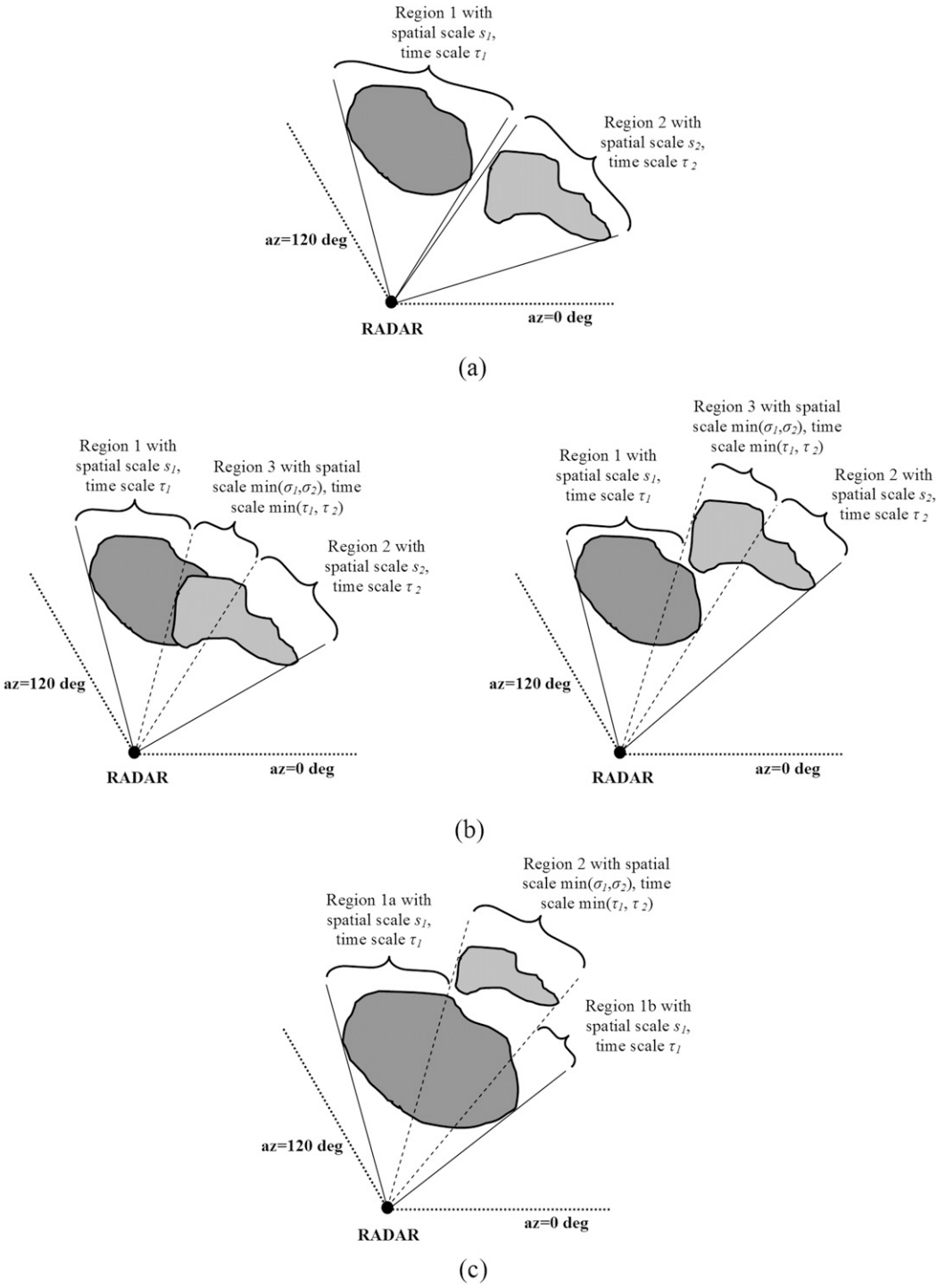

FIG. 7. Radar scanning region scheme.

and temporal scale of the overlapping region are defined as min(s_1, s_2) and min(τ_1, τ_2), respectively, where (s_i, τ_i) are denoted for spatial and temporal scales of region *i*th, respectively. If the spatial and temporal scales of the overlapping region are different from that of either existing region, then it is treated as a new scanning region. A similar approach is used for the case of the completely overlapping category (Fig. 7c). If the space–time scales of the smaller region are equal to or larger than that of the larger region (region 1), then we do not

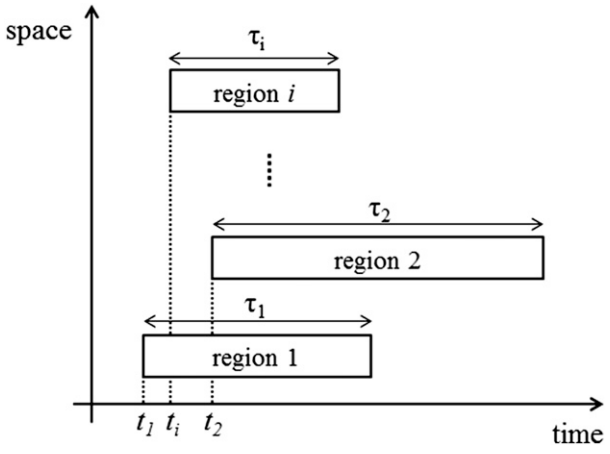

FIG. 8. The space–time diagram of radar scanning regions.

care about the smaller region and it can be removed from the scheme. Otherwise, it creates a new scanning region and the larger region is split into two separate regions (region 1a and region 1b) with the same space–time parameters.

Once all the scanning regions are specified, their space–time diagram can be generated. In general, scanning regions may begin at different time stamps and have different evolution times. Figure 8 depicts this idea. Knowing the space–time diagram helps the radar scheduler optimize the scan with the goal of accurately capturing more features from the storm.

4. Measurement error model

In designing the PAWR scan strategy, the measurement error model is an important element. Many factors need to be considered, such as the accuracy of the signal spectral moment estimates (mean power, mean Doppler velocity, and signal spectrum width) and the performance of ground clutter filtering for weather application. In this work, for the sake of simplicity, we use a measurement error model based on the accuracy of the mean power estimates and the signal-to-noise ratio (SNR) is sufficiently large so its inverse is negligible and can be omitted from the standard deviation equation of the mean power (Doviak and Zrnić 1993). This keeps the work focused on the main objective, which is the use of the space–time characterization model for PAWR scan strategy.

a. Case of no clutter

Let us first consider the case without ground clutter contamination. For this case, signal power is estimated as the mean of instantaneous power samples (Bringi and Chandrasekar 2001). The number of samples determines the accuracy of measurement. In the ideal case where the signal samples are independent, the variance of the mean power estimate is computed as (Bringi and Chandrasekar 2001)

$$\mathrm{var}(\hat{\overline{P}}) = \frac{(\overline{P})^2}{m}. \tag{8}$$

The received signal is often express in decibel (dB) scale, and the standard deviation of the mean power estimate (dB) is given by

$$\mathrm{std}[\hat{\overline{P}}(\mathrm{dB})] \approx 10\log_{10}\left[1+\frac{\mathrm{std}(\hat{\overline{P}})}{\overline{P}}\right] = 10\log_{10}\left(1+\frac{1}{\sqrt{m}}\right), \tag{9}$$

where m is the number of samples. For example, we need only $m = 15$ independent samples to achieve $\mathrm{std}(\hat{\overline{P}}) = 0.99$ dB. However, if the precipitation signals are correlated, then a larger number of samples are required to obtain the same statistical variance. It is known that the standard deviation of the signal power estimates is a function of the number of samples and the signal spectrum width (σ_p). For a given number of samples, the variance of power estimates increases with the decreasing spectrum width (Bringi and Chandrasekar 2001). This is because the signal decorrelation time is larger at smaller spectrum widths; therefore, the equivalent number of independent samples is smaller. In this work, the decorrelation time T_d of the medium is defined as the time for the signal autocorrelation function to fall to 0.01 instead of e^{-1} as in Bringi and Chandrasekar (2001). Thus, it is derived in a similar way and is expressed as

$$T_d = \frac{2.146\lambda}{2\sqrt{2}\pi\sigma_p}, \tag{10}$$

where λ is the radar wavelength and σ_p is the signal spectrum width.

As mentioned above, PAWR can instantly steer the beam to scan and revisit a region. This capability of PAWR permits a new pulsing scheme in order to reduce the scan time without compromising the accuracy of the radar measurements. The pulsing scheme for PAWR is shown in Fig. 9. In this scheme, PAWR transmits and receives a block of a small number of pulses, denoted by m_i for regions ith, and revisits that region after time T_i. The revisit time (or update time) T_i is sufficiently large such that the signals from adjacent blocks are uncorrelated. During the revisit time, the radar beam of PAWR is steered within the other regions of interest to collect samples at many beam locations. A block size

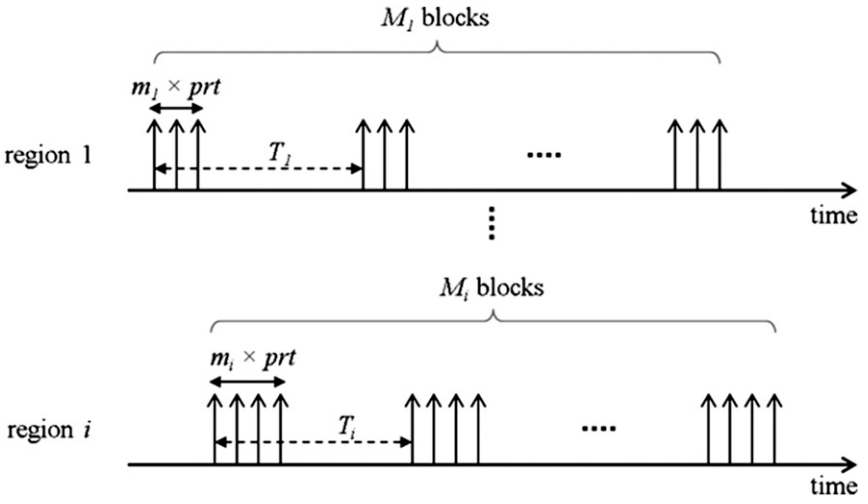

FIG. 9. Block pulsing scheme for PAWR.

$m_i \geq 2$ is required for the estimation of mean Doppler velocity and spectrum width [beam multiplexing (BMX); Yu et al. 2007). It is favorable to choose a block size (m_i) as small as possible to reduce the scan time; however, m_i needs to be sufficiently large to allow for implementing a clutter filtering algorithm (section 4b). In addition, a large block size will increase the number of pulse pairs for Doppler processing, thus improving the standard deviation of Doppler velocity estimates over the BMX method (Yu et al. 2007).

Next, we will examine the statistical errors of the power estimates for the block pulsing scheme. The variance of the mean power estimate from a block is given as (Doviak and Zrnić 1993)

$$\mathrm{var}(\widehat{\overline{P}}) = \frac{(\overline{P})^2}{m_i} \sum_{l=-(m_i-1)}^{(m_i-1)} \left(1 - \frac{|l|}{m_i}\right) \rho_p(l), \qquad (11)$$

where $\rho_p(l)$ is the correlation coefficient of weather signal at lag l. When M_i blocks are independent, the variance of the mean power estimate is

$$\mathrm{var}(\widehat{\overline{P}}) = \frac{(\overline{P})^2}{M_i m_i} \sum_{l=-(m_i-1)}^{(m_i-1)} \left(1 - \frac{|l|}{m_i}\right) \rho_p(l). \qquad (12)$$

Figure 10 shows the standard deviation in estimated powers using the simulation for an S-band radar. In this example, the block size varies from 4 to 32 and σ_p is chosen between two values representing narrow ($2\,\mathrm{m\,s^{-1}}$) and wide signal spectra ($4\,\mathrm{m\,s^{-1}}$). The parameters are estimated using the autocovariance method. White lines are theoretical curves derived from Eq. (12) for the standard deviation of power estimates 1 and 2 dB. The analysis aids the design stage of selecting a combination of block size and number of independent blocks to achieve the desired measurement accuracy. For example, at spectrum width of $4\,\mathrm{m\,s^{-1}}$ and a block size of 4, we need 10 blocks (i.e., 40 samples) to achieve a standard deviation of estimated mean power less than 1 dB, while for conventional weather radar at least 64 samples are needed to obtain a similar performance.

b. *Case of clutter contamination*

Ground clutter filtering is critically important for improving the radar data quality of any weather radar system. If not removed, the clutter may produce strongly biased estimates of the fundamental spectral moments, such as mean power, mean Doppler velocity, and spectrum width. For PAWR, the ground clutter issue is even more vital because the phased array antenna beamwidth and sidelobe-level performance are generally not as good as that of the parabolic antenna, and it becomes even worse when the beam is directed off boresight. Therefore, PAWR demands a filter with a better clutter suppression ratio. Additionally, in the PAWR block pulsing transmission scheme (Fig. 9), the received signal is not continuously sampled. In fact, it consists of many independent blocks with fewer samples, so classical clutter filtering methods will not work on this type of data. Nguyen and Chandrasekar (2013) introduced a new ground clutter filtering method [Gaussian model adaptive processing in the time domain (GMAP-TD)] that provides excellent performance even in cases of strong ground clutter contamination. In this section, we will extend the GMAP-TD algorithm to PAWR block data.

In designing the GMAP-TD algorithm, the size of the covariance matrix is configurable. This is a very important feature of the GMAP-TD filter because it opens up the possibility to adapt this filter to work in PAWR

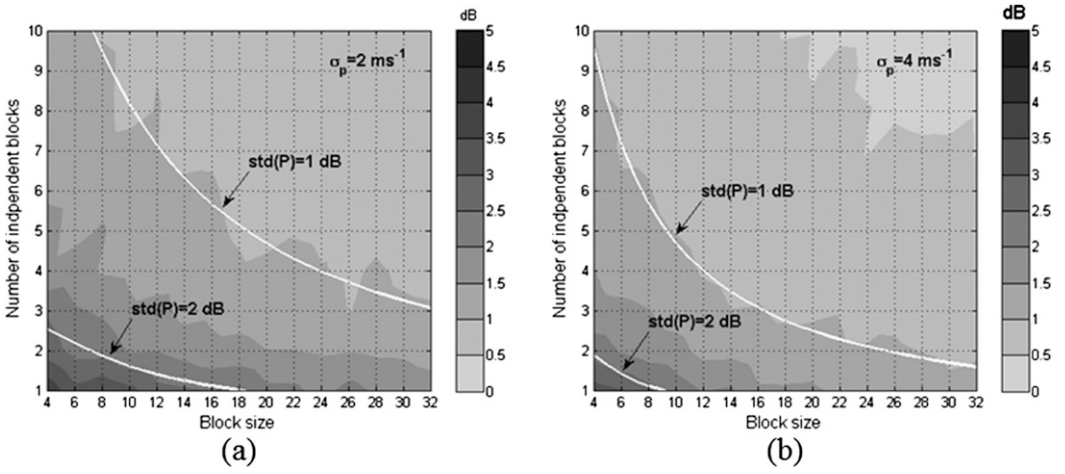

FIG. 10. Standard deviations of power estimates as a function of block size and number of independent blocks with two spectrum width values: (a) $\sigma_p = 2\,\mathrm{m\,s^{-1}}$ and (b) $\sigma_p = 4\,\mathrm{m\,s^{-1}}$.

block pulsing mode. A signal covariance matrix is generated from each block of length m_i and then is averaged over all blocks. This helps to reduce the variance of the average covariance matrix and therefore improves the performance of the GMAP-TD filter. In fact, the four factors determining the filter performance are SNR, block size, number of independent blocks, and ground clutter level. For example, for a given clutter-to-signal ratio (CSR), the same performance can be achieved by either using a larger block size or increasing the number of blocks. These factors are trade-offs and need to be considered when designing the waveform for PAWR. Next, the performance of the GMAP-TD filter is evaluated with different combinations of block size, number of blocks, and CSR using simulations. In all cases, the SNR is set at 20 dB. Input parameters for the simulation are given in Table 1. A standard deviation of power estimates is used to gauge the filter performance. The first analysis is done by fixing CSR and varying the other factors. Low CSR (20 dB) and moderate CSR (40 dB) are used and the results are shown in Figs. 11 and 12, respectively. White contour lines are superimposed at std(P) = 1 dB and std(P) = 2 dB. It can be seen that the GMAP-TD filter works well even with a small block size. In most situations, six blocks of eight samples would provide std(P) $\leq$ 1.5 dB. In an extreme case, where CSR = 40 dB and the spectrum width is as small as $2\,\mathrm{m\,s^{-1}}$, a block size of 10 is required to obtain std(P) $\leq$ 1 dB. In the second analysis, we study the performance of the GMAP-TD filter at various CSR levels (Fig. 13) while the block size is fixed at 8. Apparently, to retain the same performance, more blocks are required when CSR is increasing. If the accuracy requirement is 1.5 dB $\leq$ std(P) $\leq$ 2 dB, then the method needs a relatively small number of blocks (e.g., eight blocks when $\sigma_p = 2\,\mathrm{m\,s^{-1}}$ and only six blocks when $\sigma_p = 4\,\mathrm{m\,s^{-1}}$). If a highly accurate measurement [std(P) = 1 dB] is required at CSR = 40 dB and a small spectrum width ($\sigma_p = 2\,\mathrm{m\,s^{-1}}$), then using a block size larger than eight is recommended (Fig. 13a).

5. Design of scan strategy for PAWR

a. Adaptive scanning strategy

In designing the scan strategy for PAWR, the space–time characterization model plays a key role. It handles the storm motion and provides position information for radar scanning regions and their space–time variability parameters. Quickly evolving regions need to be scanned more often than slowly evolving regions and the scan needs to be complete within the evolution time. In addition, regions with larger spatial scale can be sampled at coarse resolution, while regions with smaller scales need to be scanned using a finer resolution. Moreover, the measurement error model provides information about the number of independent samples that must be collected at each beam location to achieve good data. As a result, data quality and acquisition time can be

TABLE 1. Radar simulation input parameters.

Parameters	Values
f (GHz)	2.72
CSR (dB)	20, 40
SNR (dB)	20
σ_p (ms^{-1})	2, 4
Block size (samples)	1, 8
PRT (ms)	1.0

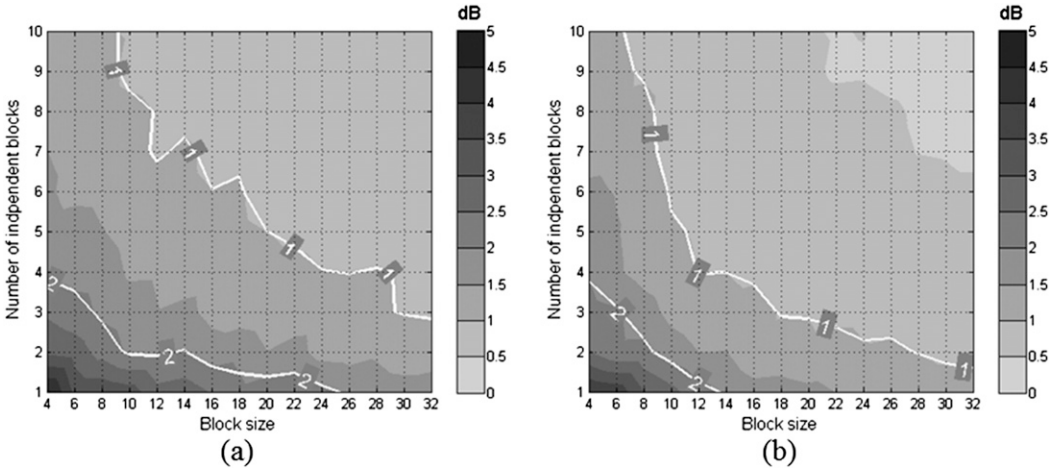

FIG. 11. Standard deviations of power estimates as a function of data block size and number of blocks with CSR = 20 dB, and two spectrum width values: (a) $\sigma_p = 2\,\mathrm{m\,s^{-1}}$ and (b) $\sigma_p = 4\,\mathrm{m\,s^{-1}}$.

optimized. This is a fundamental framework of an adaptive scan strategy as proposed in this paper. However, the scan strategy will not be complete without addressing the following considerations.

1) REVISIT TIME CONSTRAINTS

The revisit time or update time illustrated in Fig. 9 is specified for each scanning region during scheduling to minimize scan time. The requirements of independent samples and fast scan put constraints on the revisit time. While it is desirable to have a large revisit time to obtain independent samples, the scan has to be completed within the evolution time of the event. The revisit time may or may not satisfy both conditions. To examine this issue, let us consider an extreme scenario where an S-band PAWR is scanning a rapidly evolving region such that the area around the tornado vortex (Fig. 4) has an evolution time of 0.145 min, or 8.7 s. Assuming the signal spectrum width is as small as $1\,\mathrm{m\,s^{-1}}$ at that region, the revisit time should be equal to or larger than 24.2 ms [Eq. (11)] to get independent samples. Thus, in this case we are able to collect 270 independent blocks of eight samples that provide an estimated power with a standard deviation less than 1 dB (Fig. 10). For most meteorological applications, this level of accuracy is adequate (ROC 2007). Therefore, it is assured that when we constrain the total scan time to be equal to the estimated evolution time, the average revisit time will be equal to or larger than the signal decorrelation time. Thus, for each scanning region we define the lower boundary of the revisit time as the signal decorrelation time, and the following procedure provides the upper

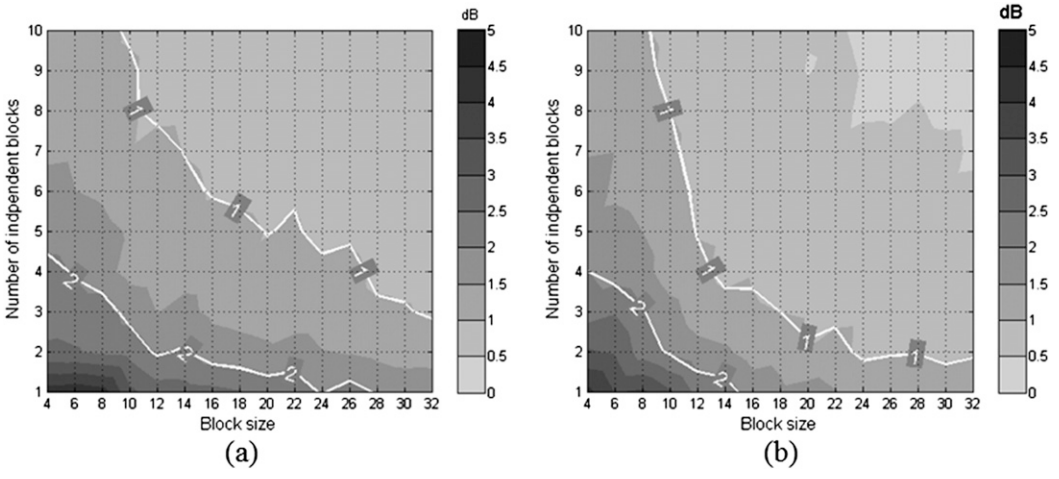

FIG. 12. As in Fig. 11, but for CSR = 40 dB.

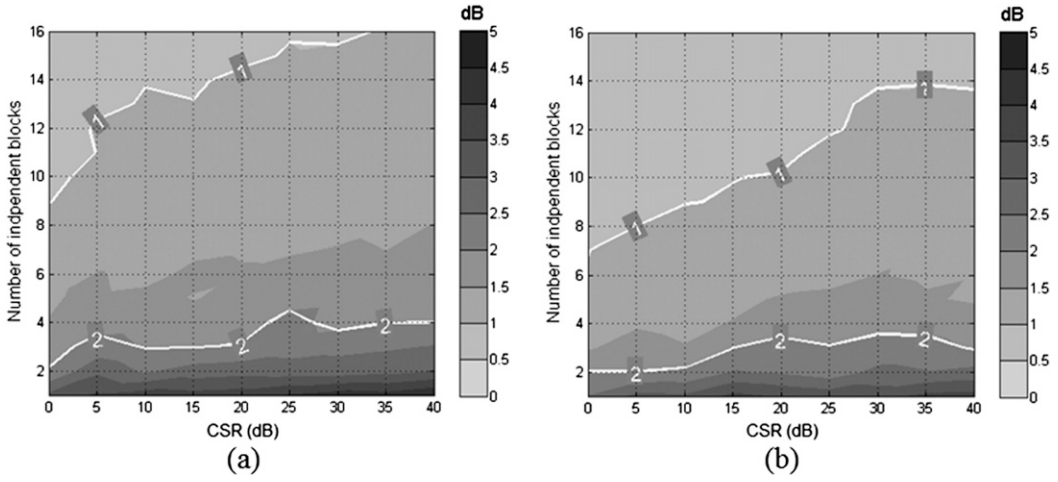

FIG. 13. Standard deviations of power estimates as a function of CSR and number of blocks with a block size of 8, and two spectrum width values: (a) $\sigma_p = 2\,\mathrm{m\,s^{-1}}$ and (b) $\sigma_p = 4\,\mathrm{m\,s^{-1}}$.

boundary: 1) given the block size and level of data accuracy, specify a number of independent blocks (M_i) based on the measurement error model (section 4); and 2) divide the evolution time by M_i to obtain the upper boundary of the revisit time. The revisit time will then be selected within this interval to produce an optimal scan.

2) IMPROVED ADAPTIVE SCANNING WITH NOWCASTING

Adaptive scanning strategies imply that the radar is able to adjust the beam location to regions of weather phenomena as they are predicted to develop. Hence, short-term prediction (nowcasting) needs to be integrated into the scan strategy to improve radar observations. The predicted reflectivity field provides information on the future position of a moving storm and then this information is used to adjust the scan strategy to observe the entire storm. This is very important, especially when tracking or scanning a fast-moving storm. The capability of this strategy is demonstrated in Fig. 14. Figure 14 depicts an image of a Collaborative Adaptive Sensing of the Atmosphere (CASA) radar display on 17 May 2009, comparing coverage afforded by radar node steering using previous observation versus steering using a 5-min prediction (Ruzanski et al. 2011). In this case, the storm was moving toward the northeast. It can be seen that the leading edge is observed when prediction information is used in scan strategy and is missed when it is not used. Although Fig. 14 is from an X-band radar network, this strategy can be extended to any other ground weather radar systems at different frequency bands, including S-band phased array weather radars.

3) WAVEFORM SELECTION

The waveform selection process addresses the selection of adequate waveforms from a waveform database for each radar scanning region. Primarily, this ensures selecting the correct waveform and signal processing to match the requirements of maximum unambiguity range, maximum unambiguity velocity, range resolution, and measurement sensitivity. For surveillance tasks, the radar may use a set of two predefined waveforms: one for longer range measurement and one for high Doppler velocity measurement. For the main tasks, the choice of waveform depends on the storm's parameters at beam position and the goal of the measurement. Available waveforms are uniform pulse repetition time (PRT), batch PRT, and staggered PRT.

In summary, the flow diagram of the adaptive scan strategy for PAWR is shown in Fig. 15.

b. Scheduler requirements

In this work the scan strategy algorithm for PAWR is designed to work on a ray-to-ray basis. Each ray is considered as a task, and the dwell time of the task (or *task time*) is equal to the length of the block of pulses at that ray. All tasks are competing for radar resources (time and hardware); therefore, effective resource management is required for a successful operation. The central part of resource management is a scheduler that arranges the tasks in a sequence without significant delays. The requirements for a real-time scheduler for PAWR can be summarized as follows:

1) Determine in real time a sequence of beam position in which the sampling time at each position is conditioned by the accuracy of measurement.

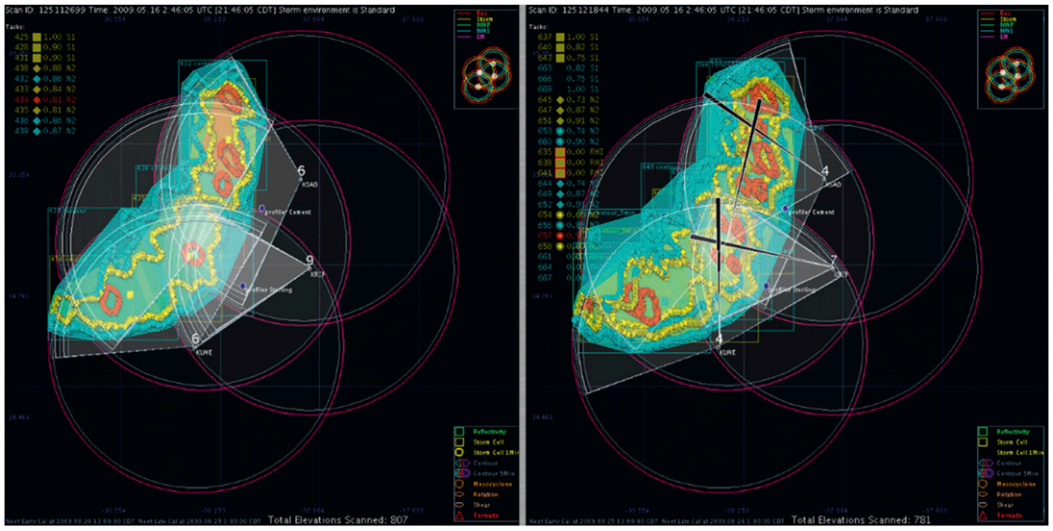

FIG. 14. Example demonstrating the importance of incorporating nowcasting into the scan strategy. Images from the CASA radar display on 17 May 2009, comparing coverage obtained by radar nodes steering using (left) previous observations vs (right) adaptive scanning using 5-min nowcasts (Ruzanski et al. 2011).

2) Follow a priority structure for the revisit times according to the evolution of different storm regions.
3) Minimize the scan time to obtain high-temporal-resolution observation of the storm.
4) Allow implementation of adaptive waveform control according to different types of storms.
5) Maintain the angular separation between two consecutive beam positions to suppress high-order (e.g., second) trip echo from the previous beam position.
6) Balance scanning time and surveillance time.
7) Fully use the antenna/radar resources.

c. *An algorithm for task scheduling in PAWR*

In this section we present an algorithm that arranges a sequence of the tasks based on the tasks' priority and an approach to optimize the radar scan time. The algorithm works similarly to the time balance scheme to control

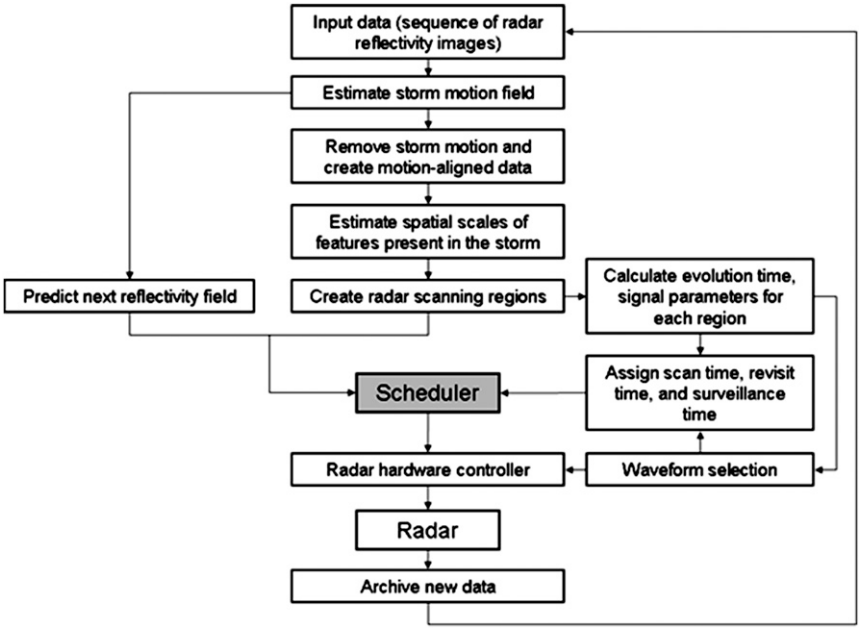

FIG. 15. Flowchart of PAWR adaptive scan strategy algorithm.

TABLE 2. Space–time parameters of the radar scanning regions.

	Azimuthal range (°)	Azimuthal resolution (°)	Evolution time (min)	Spectrum width ($m\,s^{-1}$)
Region 1	31–65	1	0.15	4
Region 2	70–100	2	0.30	2

the scheduling of tasks as in the work of Stafford (1990). The time balance concept was first introduced for military applications and recently was extended for use in the application of phase array radar for tracking multiple storms (Reinoso-Rondinel et al. 2010). A scheduling algorithm using the time balance scheme is summarized as follows:

1) Each task is associated with a time balance variable.
2) A positive time balance means the task is late for execution. The task with the highest time balance value has the highest priority.
3) When a task is finished, the time balance of all the tasks is increased by the task time. Then, the time balance variable associated with this task will be decreased by its revisit time.
4) Steps 1–3 are repeated.

In addition to the main tasks, a surveillance task is included in the scan strategy. When a surveillance task is triggered, the radar will scan the nonprecipitating regions at a rate that depends on the requirement of data quality. The number of such regions defines the number of surveillance tasks. The surveillance task time is defined as the time needed by the radar to scan the entire surveillance area continuously. The update time of a surveillance task is provided by the user. For example, the user can assign a high surveillance update time to important and potentially hazardous storms and a low update time to other storms. Usually, the surveillance task time and the update time are much longer than the task time of scanning a ray. A surveillance task is executed when it is at the highest priority level or when the time balance of all the main tasks is negative. In other words, surveillance runs when it is requested or when radar resources are available.

As can be seen from the scheduler algorithm, changing the update times of tasks will produce different results. The question is how to choose the revisit times to obtain optimal results and to avoid an overloading problem for PAWR. In section 5a(1), we have proposed a method for finding the constraints for the revisit time at every scanning region. Each visit time is constrained in a specific interval. In general, there is no closed-form expression for this optimization problem, since the conditions vary from case to case. Any attempt to change the update times while scheduling tasks will exacerbate the complexity of the algorithm. We approach this problem in a traditional way: by considering all possible input combinations. To do this, each revisit time is scanned within its interval with the increment of radar PRT (normally on the order of milliseconds) and then the combination that provides the smallest scan time result is chosen. Because the scheduler algorithm is fairly simple, this solution works well as demonstrated in the next section.

d. *The scheduler performance evaluation using simulation*

To demonstrate the advantage of PAWR, a simple example of scheduling scanning tasks for a storm consisting of two separate radar scanning regions is presented. One region represents the quickly evolving (e.g., convective) part of the storm. The other represents the slower developing region (e.g., stratiform) part of the storm. The regions' locations are shown in Fig. 7a. We assume that PAWR antenna beamwidth can be configured to match with the region spatial resolutions. At the region where smaller spatial scales are present the antenna pattern is formed to have a narrow beamwidth, and at a region with a large spatial scale the antenna pattern is synthesized with a wider beamwidth (in this case, 1° or 2°). It is noted that when the PAWR beamwidth increases, the antenna gain diminishes, since it is inversely proportional to the product of azimuth and elevation beamswidths. Consequently, the SNR will drop by 6 dB in the large-scale region if the beamwidth increases from 1° to 2°. As mentioned before (section 4), in this work we assume that the SNR is sufficiently large so the drop in SNR does not affect the analysis of the measurement error model. In practice, the SNR needs to be considered and the scheduler algorithm has to account for the change in SNR when forming the antenna's beam. Based on the SNR information of the scanning region (this can be obtained from a surveillance scan or a previous scan), the scheduler determines the beamwidth of PAWR to minimize the dwell time in that region. Details on this topic are beyond the scope of this paper.

The space–time parameters of the two regions generated by the characterization model are given in Table 2. Additionally, we assume that the requirement of minimum angular separation between two consecutive PAWR beam positions is 6° to avoid the effect of the high-order trip echo from the previous beam position. One scan will complete when it achieves std(P) = 1 dB or better at all azimuth locations. We will compare the scan time of PAWR with that of a conventional weather radar (CWR) with a 1° beamwidth antenna. Also, no surveillance task is

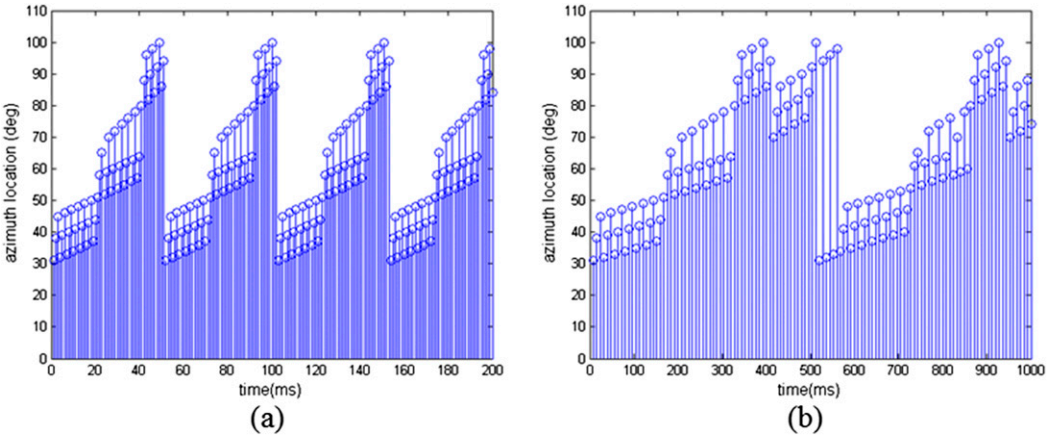

FIG. 16. Schedule beam positions for cases with a block size of (a) 1 and (b) 8.

scheduled in this example. Two pulsing schemes are studied as follows:

1) CASE 1: BLOCK SIZE OF ONE FOR BOTH REGIONS

Clearly, this pulsing scheme will provide the fastest scan speed but no Doppler velocity or spectrum width. Using the method proposed in section 5a(1), we compute the revisit time intervals for regions 1 and 2: (6, 600) and (12, 1200) ms, respectively. We try all the combinations for the two revisit times (in this case the time increment is 1 ms); the revisit times $T_1 = 10$ ms and $T_2 = 12$ ms provide the smallest scan time. With this setting, PAWR is able to finish scanning the whole storm (Fig. 7a) in only 0.835 s. The final scheduled tasks (beam positions) in the first 200 ms of the scan are shown in Fig. 16a. In contrast, a conventional radar with a 1° beamwidth antenna requires 105 samples [Eq. (12)] at each azimuth location to obtain $\mathrm{std}(\widehat{P}) \leq 1$ and therefore takes 7.35 s (105 ms × 70 rays) to finish this sector (from azimuth 31° to 100°).

2) CASE 2: BLOCK SIZE OF EIGHT FOR BOTH REGIONS

Increasing the block size will increase the scan time, but it also provides Doppler velocity and spectrum width estimates and more importantly, it allows the implementation of a ground clutter filtering algorithm (section 4b) if required. Hence, this scheme is more practical for normal radar operation. From the measurement error model (Fig. 10), we need to collect at least six independent blocks at each beam position for region 1 (spectrum width: 4 m s^{-1}) and 10 independent blocks at each beam position for region 2 (spectrum width: 2 m s^{-1}). In this case, the upper boundary for revisit times (in order to meet the requirement of evolution time) for the two regions are 1285 and 1800 ms, respectively. The revisit time intervals for regions 1 and 2 are (6, 1285) ms and (12, 1800) ms, respectively. Again, by scanning all the possible combinations for the revisit times, we calculate values of $T_1 = 20$ ms and $T_2 = 12$ ms that provide a minimum scan time of 2.96 s. The scheduled beam positions for the first 1000 ms are depicted in Fig. 16b.

Figure 16 shows that by using this strategy, the scan time can be optimized while all the tasks are executed (no overloading problem). Besides the total scan time, scheduling parameters, such as the number of schedule tasks at each beam location and the total task time, are summarized in Table 3.

6. Summary and discussion

Phased array weather radar has the potential to provide fast updates that can help increase warning lead

TABLE 3. Scan strategy algorithms' outputs. Results for the total scan time are set in bold.

	Block size of 1		Block size of 8	
	CWR	PAWR	CWR	PAWR
No. of block/block size (samples) for region 1	1/105	15/1	1/105	6/8
No. of block/block size (samples) for region 2	1/105	15/1	1/105	10/8
Total scan time (s)	**7.35**	**0.765**	**7.35**	**2.96**
std(P) for region 1 (dB)	0.99	0.99	0.99	1.00
std(P) for region 2 (dB)	0.73	0.99	0.73	0.95

times and to better understand quickly evolving weather phenomena. To make full use of radar resources and to achieve optimal observations, a scanning strategy must be addressed. In this paper, a new concept of adaptive scanning strategy for PAWR has been introduced for this purpose. The adaptive sensing framework is based on the space–time variability feature of the storm. It is suggested that regions with smaller spatial scales tend to evolve more quickly than regions with larger scales and therefore need to be updated more often. To validate this hypothesis and to estimate qualitative parameters, a new space–time characterization model for precipitation systems is developed. The system includes 1) an algorithm for scale detection and estimation, 2) a characterization model, and 3) a scheme for mapping space–time parameters into radar scanning regions. The scale estimation algorithm detects the significant changes in similarity measurements of the observation and its filtered outputs. Using a model simulation, it is demonstrated that the algorithm performs well with radar reflectivity data. A space–time characterization model that explicitly includes the interaction between space and time has also been presented and evaluated. The storm evolution process over time is characterized by a kernel dilation model after the storm motion pattern is removed. To preserve the signal spatial characteristic, each kernel is approximated by summation of many isotropic Gaussian kernels whose scales are extracted from all observations in the sequence. The weight factors of the kernels are then thresholded and mapped into regions termed radar scanning regions. The model has been tested on simulated radar data. The results are consistent with our space–time variability hypothesis.

Next, a new pulsing scheme solely developed for PAWR and an associated measurement error model are introduced. In this scheme, a radar beam will be rapidly steered within the scanning regions to collect blocks of a small number of samples and revisited after certain intervals. A block size from 2 to 8 is chosen depending on the clutter level at beam position. The measurement error model is used to determine whether the data quality requirement is satisfied.

Last, the design of the adaptive scan strategy is presented. Within the strategy, many aspects have been considered and discussed, such as calculation of revisit time constraints, incorporation with nowcasting to improve observation, spatial sampling adaptation, and waveform selection. All these considerations provide critical inputs for the scheduler that is responsible for scheduling all radar tasks. A scheduling algorithm based on the time balance concept is used in this work. Additionally, a procedure to optimize the selection of revisit times for scanning regions is also presented. The scheduler algorithm is demonstrated to be stable and the computation is very efficient. The occupancy is very high owing to the small task time (equal to block size). As a result, PAWR can significantly reduce the scan time while maintaining the data quality required by conventional weather radar. Moreover, the designed scan strategy allows PAWR to accurately capture storm features within their evolution times.

Acknowledgments. This work was inspired by the National Science Foundation (NSF) CASA Engineering Research Center (ERC) program. The research work is supported by CSU Research Foundation (EDA 14-245). The authors thank Professor Greg Tripoly for providing high-resolution model results used in this paper.

REFERENCES

Bringi, V. N., and V. Chandrasekar, 2001: *Polarimetric Doppler Weather Radar: Principles and Applications*. Cambridge University Press, 636 pp.

Doviak, R. J., and D. S. Zrnić, 1993: *Doppler Radar and Weather Observations*. 2nd ed. Academic Press, 562 pp.

Gang, X., and V. Chandrasekar, 2005: Radar storm motion estimation and beyond: A spectral algorithm and radar observation based dynamic model. *Symp. on Nowcasting and Very Short Range Forecasting (WSN05)*, Toulouse, France, World Weather Research Programme and Météo-France, 2.41. [Available online at http://www.meteo.fr/cic/wsn05/resumes_longs/2.41-138.pdf.]

Heinselman, P. L., D. L. Priegnitz, K. L. Manross, T. M. Smith, and R. W. Adams, 2008: Rapid sampling of severe storms by the National Weather Radar Testbed Phased Array Radar. *Wea. Forecasting*, **23**, 808–824, doi:10.1175/2008WAF2007071.1.

Lawson, C. L., and R. J. Hanson, 1987: Linear least squares with linear inequality constraints. *Solving Least Squares Problems*, Society for Industrial Mathematics, 158–173.

National Research Council, 2009: *Observing Weather and Climate from the Ground Up: A Nationwide Network of Networks*. National Academies Press, 250 pp., doi:10.17226/12540.

Nguyen, C. M., and V. Chandrasekar, 2013: Gaussian model adaptive processing in time domain (GMAP-TD) for weather radars. *J. Atmos. Oceanic Technol.*, **30**, 2571–2584, doi:10.1175/JTECH-D-12-00215.1.

Park, J., and I. W. Sandberg, 1991: Universal approximation using radial-basis-function networks. *Neural Comput.*, **3**, 246–257, doi:10.1162/neco.1991.3.2.246.

Rasmussen, E. N., S. Richardson, J. M. Straka, P. M. Markowski, and D. O. Blanchard, 2000: The association of significant tornadoes with a baroclinic boundary on 2 June 1995. *Mon. Wea. Rev.*, **128**, 174–191, doi:10.1175/1520-0493(2000)128<0174:TAOSTW>2.0.CO;2.

Reinoso-Rondinel, R., T.-Y. Yu, and S. Torres, 2010: Multifunction phased-array radar: Time balance scheduler for adaptive weather sensing. *J. Atmos. Oceanic Technol.*, **27**, 1854–1867, doi:10.1175/2010JTECHA1420.1.

ROC, 2007: WSR-88D system specification. WSR-88D Radar Operations Center Rep. OWY55, 164 pp.

Rood, R. B., 1987: Numerical advection algorithms and their role in atmospheric transport and chemistry models. *Rev. Geophys.*, **25**, 71–100, doi:10.1029/RG025i001p00071.

Ruzanski, E., V. Chandrasekar, and Y. Wang, 2011: The CASA nowcasting system. *J. Atmos. Oceanic Technol.*, **28**, 640–655, doi:10.1175/2011JTECHA1496.1.

Stafford, W. K. 1990: Real time control of multifunction electronically scanned adaptive radar (MESAR). Preprints, *IEE Colloquium on Real Time Management of Adaptive Radar Systems*, London, United Kingdom, Siemens Plessey Radar, 1–5. [Available online at http://ieeexplore.ieee.org/document/191190/.]

Tripoli, G. J., and M. L. Büker, 2012: Numerical simulation of three-dimensional vortical interactions within an idealized tornado. *26th Conf. on Severe Local Storms*, Nashville, TN, Amer. Meteor. Soc., 1.2. [Available online https://ams.confex.com/ams/26SLS/webprogram/Paper212293.html.]

Wikle, C. K., 2002: A kernel-based spectral model for non-Gaussian spatio-temporal processes. *Stat. Modell.*, **2**, 299–314, doi:10.1191/1471082x02st036oa.

Yu, T.-Y., M. B. Orescanin, C. D. Curtis, D. S. Zrnić, and D. E. Forsyth, 2007: Beam multiplexing using the phased-array weather radar. *J. Atmos. Oceanic Technol.*, **24**, 616–626, doi:10.1175/JTECH2052.1.

Zrnić, D. S., and Coauthors, 2007: Agile-beam phased array radar for weather observations. *Bull. Amer. Meteor. Soc.*, **88**, 1753–1766, doi:10.1175/BAMS-88-11-1753.